Effects of Electron and Gamma Irradiation on Dielectric, Electrical, Optical, and Ferroelectric Properties of Lanthanum Zirconate (Lzo)

Krishna Gopal Pradhan, Research Scholar,Department Of Physics, Cmj University, Jorabat, Meghalaya, India.
Dr Prince Bansal (Assistant Professor) Research Guide,Department Of Physics, Cmj University, Jorabat, Meghalaya, India.

Abstract

Future sun based cell applications require ferroelectric materials with low bandgap energies, high polarization, low misfortune, and warm dependability. Analysts have attempted numerous strategies to get such materials. This work presents a special gamma beam irradiation technique. The underlying, optical, and ferroelectric properties of lanthanum zirconate (lzo) were analyzed after gamma radiation. X-beam diffraction, underlying refinement, and Raman examination showed tetragonal perovskite structures in all examples. Morphological examination showed grain size variety and porosity. An extensive assessment of bond lengths, bond points, octahedral twists, oxygen opening, and charge pay affirmed gamma irradiation-initiated mix impacts. Illuminated examples showed oxygen opportunities utilizing electron paramagnetic resonance (EPR).. Cole diagrams show that electron bouncing increments with gamma-beam openness. After gamma irradiation, the P-E hysteresis circle showed that ferroelectric qualities might be held with a minor remainder polarization drop. P-E conduct was related with expanding gamma irradiation in the ceramics, showing a significant gamma reliance in the circles' profile. We figure the flow technique could further develop electrical gadget multifunctionality.

Keywords: effects of electron, gamma irradiation, properties of lanthanum zirconate (lzo), Ferroelectric, dielectric.

1. INTRODUCTION

Permeable and high-surface-region materials have a few nanotechnologies utilizes. These materials are being created for catalysis, partition science, atomic strainers, zeolites, cross breed optics, bioceramics, and that's only the tip of the iceberg. Permeable pottery like calcium silicates have warm, electrical, and dielectric characteristics that make them ideal for mechanical applications. CaSiO3 can be utilized to make radio pottery, clean parts, porcelain, lining blocks, coating, and motion. The clinical business involves CaSiO3 earthenware production as biomaterials. Various techniques have orchestrated and described CaSiO3 in different stages. These materials' dielectric and electrical attributes are still inadequately perceived. Understanding dielectric and electrical qualities is urgent for applications. These materials are in many cases used in radiation-rich conditions including space, reactors, and waste holders. Radiation causes underlying modifications that change their actual properties. Hence, understanding how ionizing radiation influences these materials is critical.

Lanthanum zirconate (lzo) has gathered consideration for its extraordinary and riveting characteristics contrasted with mass materials. From naturally visible to mesoscopic scales, materials stray from mass qualities. Structures into lower aspects have a wide extension. In electron repression, excitation, emanation, ballistic conductance, and single electron burrowing depend on size. Because of their far-reaching use as interconnects and basic parts in nanoscale optoelectronic and other electronic gadgets, 1D nanostructures have been concentrated on in the new 10 years. The wires have novel and invigorating nano-level highlights contrasted with mass state: immense viewpoint proportion, exceptionally pressed electronic states, size-subordinate bandgap, and expanded surface electron and phonon dissipating. Nanowires are helpful in many fields. Semiconductors, p-n intersection diodes, energy units, supercapacitors, diodes, Li-particle batteries, sun-oriented gadgets, field outflow shows, and electrical gadget interconnects use nanowires. Limited bandgap lead chalcogenides PbZ (Z = S, Se, and Te) are concentrated on in semiconductor research in light of the fact that to their particular physico-compound, optical, and electrical highlights contrasted with III-V and II-VI. At encompassing temperature, lead selenide

ROOTINDEXING
JOURNAL ABSTRACTING AND INDEXING SERVICE

INTERNATIONAL ADVANCE JOURNAL OF ENGINEERING, SCIENCE AND MANAGEMENT (IAJESM)
July-December 2023, Submitted in July 2023, iajesm2014@gmail.com, ISSN -2393-8048
Multidisciplinary Indexed/Peer Reviewed Journal. SJIF Impact Factor 2023 =6.753

shows a 0.27 eV direct tight bandgap. PbSe is utilized in different fields because of its band structure and engaging highlights. Zero-layered PbSe quantum spots can be utilized in photovoltaics and light-transmitting diodes, one-layered nanowires in electrical, optoelectronic, and field impact gadgets, and two-layered meager movies for detecting. PbSe is great for optoelectronic infrared identifiers on the grounds that to its solid infrared reaction.

2. LITERATURE REVIEW

Dubey, N., Dubey, V., Saji, J., & Kaur, J. (2020). The thermoluminescence (TL) curve of gadolinium (Gd3+) doped phosphor La2Zr2O7 (LZO) was analyzed and trapping parameters were calculated. With precise calcination and sintering temperatures, as well as Gd3+ concentration (0.1–2.5 mol %), the phosphorus was synthesized using a modified solid-state reaction method. X-ray diffraction analysis was used to document the structural properties of the phosphors produced for optimized TL concentrations. SEM analysis revealed detailed information about the specimen's morphology. The TL luminescence curve and UV dose response for phosphors were studied at different UV radiation intensities. Trapping parameters, including trapping depth, kinetic order, and frequency coefficient to optimize dopant concentration, determined using a computerized glow curve deconvolution technique were compared with experimental data. The trap model and its parameters are discussed further.

Quader, A., Mustafa, G. M., Ramay, S. M., Riaz, S., & Atiq, S. (2023). To meet the needs of energy storage and use in microelectronic systems, electrostatic capacitors have been the subject of extensive research. Pyrochlors are at the forefront of the energy storage competition due to their low loss coefficient and high energy storage efficiency. In this work, we report the synthesis of sol-gel spontaneous combustion of the La2-xGdxZr2O7 series with substitution content x = 0.0, 0.4, 0.8, 1.2, 1.6 and 2.0. By compressing the pyrochlore structure by substituting Gd at the La site, the X-ray density is increased without a corresponding phase transition. Surface adhesion and agglomeration improved as the particle size decreased and the substitution content increased. Higher Gd content is associated with greater energy storage capacity. The Gd1.6La0.4Zr2O7 composition has been shown to be very promising for use in microelectronic devices due to its low energy loss, high recoverable energy density, and normalized capacitance and efficiency. High.

Gupta, S. K., Abdou, M., Zuniga, J. P., Ghosh, P. S., Molina, E., Xu, B., ... & Mao, Y. (2019). The optical performance of nanophosphors is significantly affected by defects, doping, and particle size. Due to the existence of ionized oxygen vacancies in the band gap, undoped La2Zr2O7 (LZO) NPs showed multicolored emission under UV irradiation in this study. The influence of particle size on the structure, surface area, photoluminescence, photoluminescence, lifetime, and quantum efficiency of La2Zr2O7:

NP Eu3+ (LZOE) was also investigated. As the co-precipitation pH increased to generate the single-source precursor for molten salt synthesis of NPs, the photoluminescence production and quantum yield gradually decreased. The potential of LZOE NPs as X-ray luminescent agents is demonstrated by their emission of red light when exposed to X-rays. We used an example of a surface defect to describe the experimental results. Energy transfer from the host to the dopant (Eu3+) was also found to be beneficial in the LZOE emission spectra. For use in photoelectronicsand X-ray therapy, this research paints a clear picture of how to create highly efficient red phosphors and X-ray scintillators.

3. EXPERIMENTAL PART

Earthenware made from lanthanum zirconate (lzo) La2Zr2O7 was delivered thanks to the state's prompt action. Bismuth volatilization was offset by the addition of 2 mol% La2Zr2O7. In a mortar made of agate, the initial particles were mashed together using CH3)2CO. In the blending process, CH3(CO)2 was used in the dispersion phase. Powder was mixed and stabilised with

CH3(CO)2 to facilitate homogeneous crushing. Drying the powder mixture at 50 degrees Celsius for an hour. The dry mixture was heated in a grill at 1000 °C for 6 hours. The CH3)2CO was used to process the heat-treated powder at the high-energy ball factory for 8 hours. Green pellets were tied using PVA at a weight of 1% to create a knot that was 1 mm thick and 10 mm wide. From 500 to 1250 degrees Celsius, the second sintering phase was heated at a rate of 5 degrees Celsius per minute. The construction was densified by maintaining 1250 degrees Fahrenheit for 4 hours. The rate of cooling from hot to cold was 5 °C per minute. Cobalt-70 gamma beams were used in the study to apply -beams of varying doses. For the purposes of identification, we used a Wi-Sleuth small Raman spectrometer powered by a Nd:YAG laser operating at 532 nm. Carl Zeiss Ultra 55 FE-SEM was used to examine the microscopic detail. The X-bandEPR spectra were estimated using room temperature Bruker Elexsys E580 spectrometers. At ambient temperature, a UV-2600 was used to create an optical representation of the materials between the wavelengths of 200 and 1500 nm. An adjusted Sawyer-Pinnacle circuit was used to make ambient temperature ferroelectric predictions at 10 Hz.

4. RESULT AND DISCUSSION

In Figure 1a, we see XRD patterns for gamma-irradiated, room-temperature lanthanum zirconate (lzo) ceramics. In every case where irradiation was involved, there was only ever one tetragonal stage, with no other stages present. The tetragonal structure of standard lanthanum zirconate (lzo) was replicated in all samples by recording their XRD designs using the JCPDS data set. Neither gamma irradiation nor extensive design dispersion resulted in the formation of further steps in the creation of lighted earthenware. Top forces and pinnacle expanding due to cross section twisting were found to be the main kinds as revealed by the X-beam diffraction patterns. Over 400 Gy lit tests showed the most diffraction design variation. Figure 1d shows that they were weaker and shifted to the 2-side, indicating a decrease in unit cell volume. Changing the primary attributes and volume is possible with the knowledge of gem cross section disfigurement, as indicated in writing. Irradiation increases or decreases the amount by which ductile pressures cause twisting. The size and characteristics of the gem grid could expand or contract.As can be seen in Figure 1b, Rietveld refinement analysis of X-beam data using Fullprof software confirmed that the precious stone period of the lanthanum zirconate (lzo) test was unaffected by the radiation. R-factors Rwp, Rb, Rexp, and 2 were used to evaluate the reliability of the building. The quality of Rietveld refinement was measured by comparing the plot errors of designs that were both noticed and evaluated. The VESTA-designed unit cell for lanthanum zirconate (lzo) ceramic is depicted in Figure 1c. Figure 2a shows that Gaussian fit was applied to the top of plane to analyse the FWHM difference, which characterised grid twisting. Scherrer and Williamson-Corridor formulas were applied to FWHM from this fitting to derive the typical crystallite size and cross section strain. The outcomes are shown in Figure 2b. Variation in crystallite size and grid strain was seen in the radiation > 400 Gy example, indicating an increase in gem cross section distortion. Despite this, doping La2Zr2O7 with Bi particles was successful. Oxygen openings in nondoped La2Zr2O7 have been hypothesised in the past to mitigate the effect of Ba2+ openings.
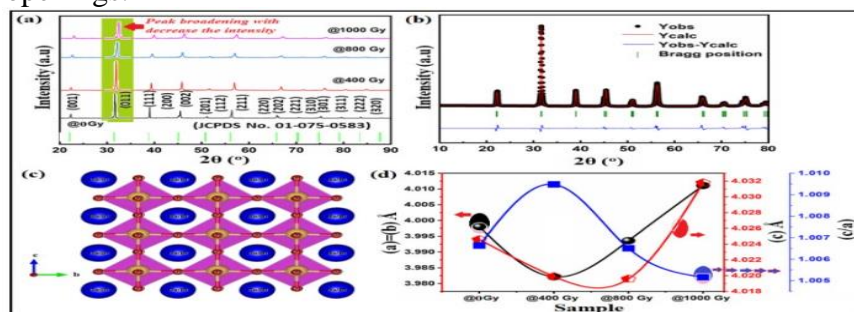
Figure 1:
(a) Example of room temperature XRD of lanthanum zirconate (lzo) clay before (thick line) &after (thick line) gamma irradiation; (b) lzo XRD refinements after calcination, with observational data shown as black circles, screening profiles shown in pink, and differences between estimated and determined diffraction patterns shown in blue. Bragg reflection at a wavelength of 4 micrometers (mm) is shown in green; (c) Structure diagram of lanthanum zirconate (lzo) gemstone for earthenware production is presented, with blue circles representing lzo, iotas, yellow circles representing Ti grains, and colored circles red represents oxygen molecules; (d) variation of the mesh constant caused by gamma particles (limit a in dark line, limit c in).
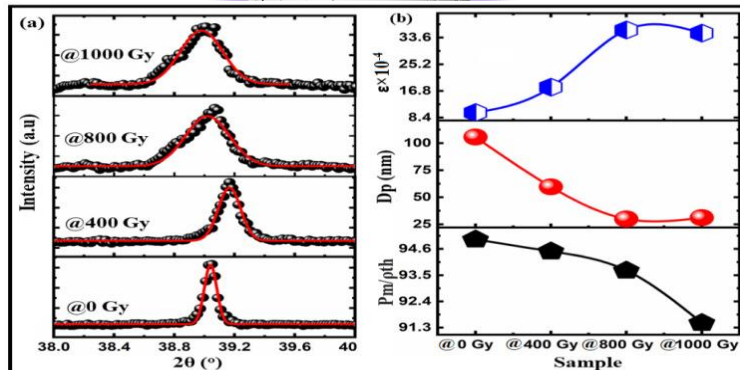
Figure 2
(a) XRD Analysis: Fit Gaussian curves to XRD data for LZO ceramics to determine lattice spacing and crystallite size.Irradiation Effects: Assess changes in crystallite size, lattice strain, and density post-gamma irradiation for LZO ceramics.

Table1: Rietveld refinement of LZO ceramics pre- and post-room temperature gamma irradiation yields insights into structural changes, including lattice parameters and atomic positions.

Sample/Parameters		@0 GY	@200 GY	@400 GY	@800 GY
Crystal structure		Tetragonal	Tetragonal	Tetragonal	Tetragonal
Lattice constant a = b (Å)		4.99801	4.98214	4.9935	5.0112
c (Å)		5.02469	5.0197	5.01963	5.0317
c/a		2.00668	2.00944	2.00657	2.005166
V (Å)^3		68.329862	68.34994	68.52532	69.20202
Space group		P5mm	P5mm	P5mm	P5mm
Space group number		98	98	98	98
Theoretical density g/cm^3		9.18	9.075	9.104	8.107
Measured density g/cm^3		9.887	9.742	8.713	7.712
Relative density (%)		96	54.6	58.8	82.6
Porosity (%)		**6**	5.6	5.4	8.6
Distortion crystal lattice (a)		-	−1.00390	1.00289	1.00435

Distortion crystal lattice (c)		-	−1.00119	-9.68×10^{-5}	1.00908
Crystallite size (nm)		235.50	82.69	81.90	40.119
Lattice strain		1.0018	1.0019	1.0038	1.0036
lanthanum zirconate (lzo),	X	0.00001	0.00001	0.00001	0.00001
	Y	1.00000	1.00000	1.00000	1.00000
	z	1.00000	1.00000	1.00000	1.00000
	Occ	2.111	2.111	2.111	2.111
	Site	2a	2a	2a	2a
	Sym	0 mm	0 mm	0 mm	0 mm
Ti/Co	X	1.60000	1.60000	1.60000	1.60000
	Y	1.60000	1.60000	1.60000	1.60000
	z	2.45632	2.87654	2.345678	2.56789
	Occ	1.135	1.298	0.97348	0.96698
	Site	3a	3a	3a	3a
	Sym	7 mm	7 mm	7 mm	7 mm
O1	X	1.60000	1.60000	1.60000	1.60000
	Y	1.60000	1.60000	1.60000	1.60000
	z	1.03864	1.06533	1.9476	1.087564
	Occ	0.765	1.365	1.7654	1.76423
	Site	2a	2a	2a	2a
	Sym	7 mm	7 mm	7 mm	7 mm
O2	X	1.60000	1.60000	1.60000	1.60000
	Y	1.60000	1.60000	1.60000	1.60000
	z	1.87654	1.65487	1.98564	1.87643
	OCC	2.289	2.453	2.5436	2.34526
	Site	1c	1c	1c	1c
	Sym	8mm	8mm	8mm	8mm
R_p%		10.8	4.62	4.85	5.12
R_{wp}%		2.95	9.54	3.82	7.83
Rex%		7.89	5.73	8.35	9.73
χ^2		1.5	1.27	1.33	1.34

Figure 1d Clearly demonstrates that the grid boundaries were expanded when gamma dose was greater than 400 Gy. Serkin D. Günay explained this anomaly by proposing the term "cross section expanding," which could be caused by deformity intergrowth. Deformities like openings may result from radiation damage aggregation in the nearby surface layer brought on by gamma irradiation. As seen in Figure 2b, the imperfection collection can result in a general thining of the

ROOTINDEXING
JOURNAL ABSTRACTING AND INDEXING SERVICE

INTERNATIONAL ADVANCE JOURNAL OF ENGINEERING, SCIENCE AND MANAGEMENT (IAJESM)

July-December 2023, Submitted in July 2023, iajesm2014@gmail.com, ISSN -2393-8048

Multidisciplinary Indexed/Peer Reviewed Journal. SJIF Impact Factor 2023 =6.753

examples. The gamma effect on the gem lattice was calculated by (1), which also provided the bending of the precious stone grid in response to variations in the gem's cross section boundaries.

Distortion crystal lattice (a) $= \frac{a_{trr} - a_0}{a_0}$ (1)

where airr and cirr are lattice constants after gamma irradiation& a0 and c0 before. Table 1 shows the parameters. Zhang et al. and Liu observed similar findings.

Raman spectra of pottery made with lanthanum zirconate (lzo) at 180-830 cm1 frequency, with Gaussian pinnacle deconvolution at room temperature, are shown in Figure 3a. Octahedral bending at the ferroelectric stage was ultimately linked to the A1(LO3) mode. The A1(TO3) mode broadened after irradiation due to mode cross-over. Figure 3 and Table 2 show that after gamma irradiation, most Raman modes change to decrease wavenumbers, possibly due to Ti cations or octahedral contortion. The situation was confirmed by the fact that gamma irradiation also decreased the power of the A1(LO3) mode.
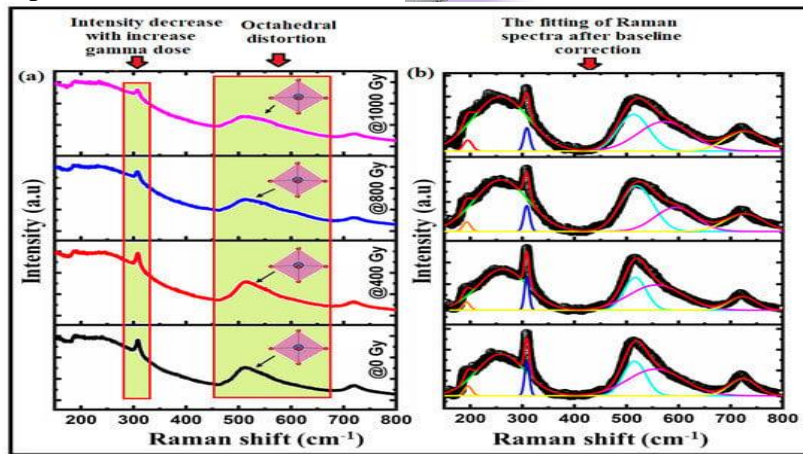
Figure 3. (a) (a) Dark line: LZO ceramic Raman spectrum before gamma irradiation. (b) Fit post-irradiation Raman spectra for analysis.

Table 2. Determined key wavenumbers and balance methods in LZO ceramics post-gamma irradiation via Raman spectra Gaussian fitting.

Modes	@0 GY	@200 GY	@400 GY	@800 GY
E(TO$_2$)	187	192	184.2	134.17
A1(TO$_2$)	243	245	253.7	243.4
E(TO$_3$)	300	305	306	355.0
A1(TO$_3$)	513	503	598.3	509
E(LO$_4$)	567	556	555	554
A1(LO$_3$)	726	727	726	710

Figure 4 shows a microstructural comparison between unirradiated and gamma-irradiated lanthanum zirconate (lzo) ceramics. Grain was distributed haphazardly, as depicted in the diagram. Large grains predominated over small ones in non-irradiated samples. After irradiation, the sample included several minute granules. After being exposed to gamma rays, the sample nevertheless retained its porosity. This demonstrates that irradiation at this dose alters the compositional consistency of the sample. Using ImageJ, the average grain size of the samples was determined. Average grain sizes were 6.977 m, 5.303 m, 4.755 m, and 4.382 m for 0 GY, 200 GY, 400 GY, and 800 GY samples, respectively. Exposure to gamma rays decreased grain size. It's possible that irradiation-induced grain fractures are to blame for this variation in typical grain size.

ROOT INDEXING
JOURNAL ABSTRACTING AND INDEXING SERVICE

INTERNATIONAL ADVANCE JOURNAL OF ENGINEERING, SCIENCE AND MANAGEMENT (IAJESM)
July-December 2023, Submitted in July 2023, iajesm2014@gmail.com, ISSN -2393-8048
Multidisciplinary Indexed/Peer Reviewed Journal. SJIF Impact Factor 2023 =6.753
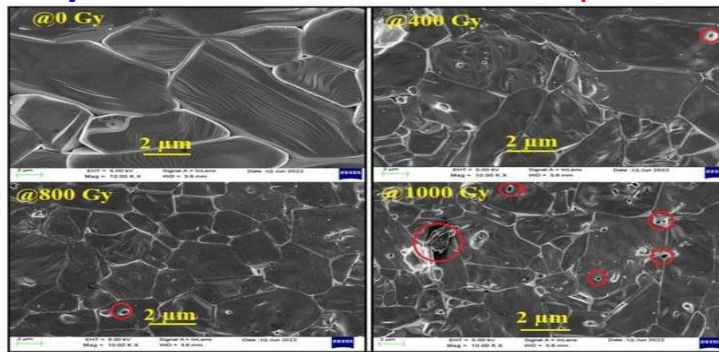
Figure 4. Scanning Electron Microscopy (SEM) of Lanthanum Zirconate (LZO) material.
Table 1 presents the results. In the ferroelectric section, we expected smaller grain size to affect polarization. Electron Paramagnetic Resonance (EPR) at room temperature tested oxygen vacancies in materials. Figure 5 displays EPR spectra for unirradiated and gamma-irradiated LZO samples (100–550 mT). Figure 5a shows no signal before irradiation. Figure 5b reveals an asymmetrical line in irradiated samples when fitted with the Lorentz function.
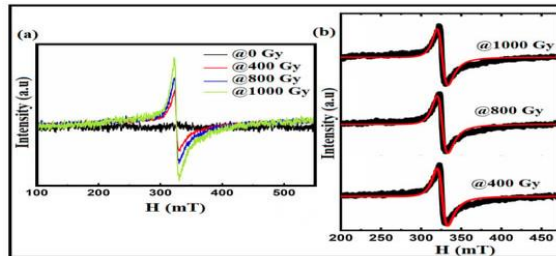
Figure 5. (a(a) Effects of radiation on EPR spectra of lanthanum zirconate (LZO) samples irradiated at 200 GY, 400 GY, and 800 GY at room temperature.(b) Lorentz fitting (red lines) of resonance spectra (dark tone) for the irradiated samples.

Figure 6a shows the estimated retention spectra of irradiated lanthanum zirconate (lzo) ceramics over the frequency range of 200-1400 nm. The sample has a retention edge in the visible spectrum before gamma irradiation, confirming a previous finding on pure BT ceramics. The red bend depicts lower energy, however for the case provided to gamma irradiation, the ingestion edge moved essentially to higher frequencies. Using a Tauc plot, we determined the direct bandgap energy of lanthanum zirconate (lzo) ceramics after gamma irradiation.

The bandgap energies of tests with gamma portions of 0 GY, 200 GY, 400 GY, and 800 GY were 3.14, 3.019, 2.89, and 2.80 eV, separately. Oxygen opening, charge pay, and octahedral contortion make sense of the apparent locale's diminished bandgap and improved ingestion range. Gamma radiation might have upgraded oxygen opening in lanthanum zirconate (lzo) earthenware production by disjoining iotas. Subsequently, radiation-uncovered earthenware production might have more oxygen opening because of dipolar complex breakdown and Compton electron barrage relocation of oxygen molecules at interstitial areas. Oxygen opening give profound or shallow contributor energy levels in the bandgap. Subsequently, the Fermi level and bandgap would change. Lanthanum zirconate (lzo) may have changed its electronic construction because of O-opening over the Fermi level. Figure 6a,b shows that this strategy expanded retention spectra and brought down bandgap energy in lighted materials..
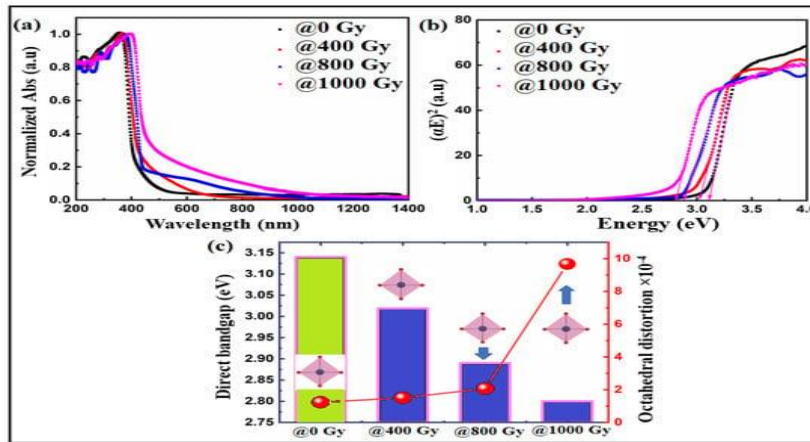
Figure 6. (a) UV-Vis absorption spectra for gamma-irradiated (dark line) and unirradiated (shaded lines) lanthanum zirconate (LZO) ceramics.(b) Tauc plot for the same materials, showing the relationship between absorption and energy.(c) Correlation between the bandgap and octahedral distortion in LZO ceramics.

$4Ba_2^{++}Ti_4^{+} \rightarrow 4Bi_3^{++}V_{Ti}$

$3Ba_2^{+} \rightarrow 2Bi_3^{++}V_{Ba}$

$Ba_2^{+} \rightarrow Bi_3^{++} e'$
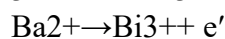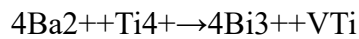
As can be seen in the red curve in Figure 6a, doping with Bi successfully increased the apparent retention power.

Finally, the bandgap energy may have been constrained due to twists in the TiO6 octahedra. The benefits of gamma irradiating lanthanum zirconate (lzo) samples, which cause them to adopt an octahedral shape, were quantified using the following equation:
:

$$\Delta d = \left(\frac{1}{6}\right) \sum_{n=1,6} [(d_n - (d))/(d)]^2$$

Individual bond distance (Ti-O) is dn, and the normal is ⟨d⟩. Table 3 shows the pre-and post-gamma octahedral contortion values for all examples. Expanded gamma portion caused mutilation. Table 3 delineates that gamma irradiation slants octahedrons, causing such distortion. Turn changed the oxygen-titanium hole, disfiguring the unit cell. Gamma irradiation might have helped cross section vibrations, giving the gem energy and causing strange octahedral variety. These variables might adjust XRD diffraction top strength and plane diffracting molecule count..

Table 3: Gamma-ray doses influence bond length, angle, octahedral distortion, and bandgap energy in materials.

Sample/Parameters	@0 Gy	@200 Gy	@400 Gy	@800 Gy
(lanthanum zirconate (lzo),-O1)×4 Å	3.83002 (9)	3.80725 (6)	3.8297 (9)	2.8679 (7)
(lanthanum zirconate (lzo),-O2)×4 Å	3.867645(6)	3.85463 (6)	3.8666 (9)	3.5377 (17)
(lanthanum zirconate (lzo),-O2) ×4 Å	3.832005 (9)	3.74335 (6)	3.8044 (9)	2.5340 (2)
(Ti-O1) Å		3.97944 (6)	2.9533 (9)	

	2.9787 (9)			2.9046 (4)
(Ti-O1) Å	3.04558(9)	3.05394 (6)	3.0491 (9)	7.1267 (9)
(Ti-O2) ×4 Å	2.9779(6)	3.9895 (6)	2.9602 (9)	3.02784 (8)
(O2-Ti-O2) deg	145.3624 (9)	155.9356 (4)	170.8488 (4)	150.637 (8)
(O1-Ti-O1) deg	282	282	282	282
Octahedral distortion $\times 10^{-4}$	3.23716	3.505409	4.066855	8.66840
Bandgap energy (eV)	3.14	3.019	2.89	2.80

Impedance spectroscopy can investigate test electrical heterogeneity by deciding grain limit commitments and limits themselves. We analyzed grain limits and obstruction during gamma irradiation utilizing complex impedance plots (Z' versus Z''). Room-temperature complex impedance range is displayed in Figure 7a. This figure shows unwinding time dissemination utilizing depressed half circles. As there were a few unwinding times, an identical equal circuit could represent the unwinding. Also, equal RQ circuits could represent unmistakable grain limit unwinding times or grain commitments. Dabbed tests show estimated information, while the red line shows an equal QR circuit model that suits it. The deliberate information was fitted to two equal RQ circuit models. Figure 7a has a similar to circuit model inset. Grain, grain limit, and cathode influences are represented by RQ components. Mass grain affected high-recurrence reactions. Grain limits and cathodes prompted low-recurrence reaction. See Table 4 and Figure 7b for subtleties. We found that gamma irradiation impacted conductivity more than impedance, bringing about a more noteworthy grain capacitance than grain limits (Ref Table 4), as expanding measurements expanded electron bouncing. The hysteresis circle changed with electron jumping, as delineated in Figure 7c. Grain limit half circles at lower frequencies were connected to ionic conduction.
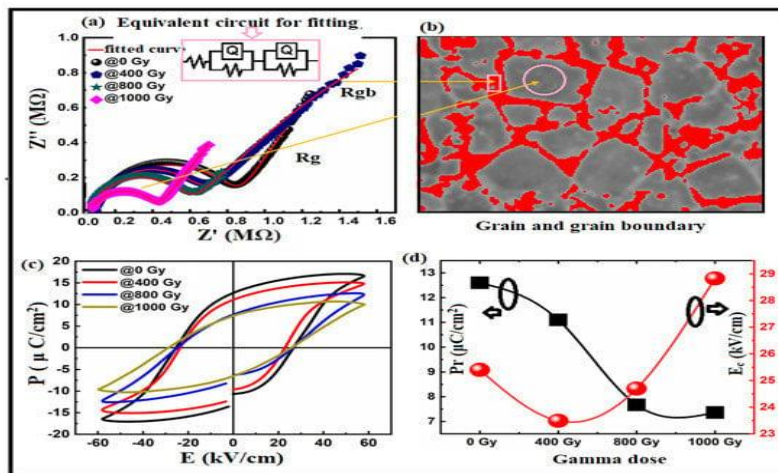
Figure 7.(a) Cole diagram illustrating room temperature gamma radiation effects on lanthanum zirconate (LZO) samples.(b) Representation of grain boundaries (dark) and grain boundaries (red) in the material.(c) Relationship between polarization and electric field for all samples.

Table 4: Results from Cole–Cole plot fitting for lanthanum zirconate (LZO) samples before and after gamma irradiation at varying doses..

	@0 GY	@200 GY	@400 GY	@800 GY
R_s (Ω)	74.34	84.57	72.43	78.54
$Q1$ (Fs^n)	4.235×20^{-5}	6.543×20^{-5}	3.489×20^{-5}	3.978×20^{-5}
R_g (k Ω)	610.8	4.789	9.543	4.876
$Q2$ (Fs^n)	3.564×20^{-7}	8.236×10^{-8}	5.455×20^{-7}	7.654×20^{-6}
R_{gb} (k Ω)	1799.9	1548.9	2522.0	1555.0

Ferroelectric P-E hysteresis circles before and after gamma irradiation are shown in Figure 7c for lanthanum zirconate (lzo), which has been heated. The graphic shows that initially there existed a circle, which may have been due to the way the samples were being maintained. Figure 7d shows that the lanthanum zirconate (lzo),ceramics had less residual polarisation after expanding the gamma section. When the gamma dose reached 400 Gy, the coercive fields shrank slightly before growing again. Increasing oxygen availability at higher radiation doses may have contributed to a decrease in Pr. There's also the possibility that the hysteresis circle behaviour was affected by the grain size and porosity.

5. CONCLUSION

solitary tetragonal stage when gamma irradiation. Raman mode movements to bring down wavenumbers following gamma irradiation were found. Morphological examination showed openings and nonuniform grain size following gamma irradiation. An extensive assessment of bond lengths, points, and octahedral mutilations laid out the gamma radiation-incited mix impact. By analysing oxygen opening, charge pay, and octahedral bending, we deduce the cause of the bandgap collapse. P-E circle conduct was related with expanding gamma portion in the ceramics, showing serious areas of strength for a reliance. We think gamma-lighted example results might be promising for electronic gadget applications.

REFERENCES

1. Quader, A., Mustafa, G. M., Ramay, S. M., Riaz, S., & Atiq, S. (2023). Tuning of efficient energy storage and fast switching capability in La2Zr2O7 pyrochlore nanoparticles mediated by Gd-substitution. *Journal of Energy Storage*, *68*, 107595.
2. Dubey, N., Dubey, V., Saji, J., & Kaur, J. (2020). Thermoluminescence glow curve analysis and trap parameters calculation of UV-induced La2Zr2O7 phosphor doped with gadolinium. *Journal of Materials Science: Materials in Electronics*, *31*(3), 1936-1944.
3. Zabaleta Llorens, J. (2015). Growth and advanced characterization of solution-derived nanoscale La Sr MnO heteroepitaxial 0.7 0.3 3 systems.
4. Gupta, S. K., Abdou, M., Zuniga, J. P., Ghosh, P. S., Molina, E., Xu, B., ... & Mao, Y. (2019). Roles of oxygen vacancies and pH induced size changes on photo-and radioluminescence of undoped and Eu3+-doped La2Zr2O7 nanoparticles. *Journal of Luminescence*, *209*, 302-315.
5. Zhao, C.; Huang, Y.; Wu, J. Multifunctional barium titanate ceramics via chemical modification tuning phase structure. *InfoMat* 2020, *2*, 1163–1190.
6. Jaffe, H. *Piezoelectric Ceramics*; Elsevier: Amsterdam, The Netherlands, 2012.
7. Lines, M.; Glass, A.M. *Principles and Applications of Ferroelectrics and Related Materials*; Oxford University Press: Oxford, UK, 1977.

8. Haertling, G.H. Ferroelectric ceramics: History and technology. *J. Am. Ceram. Soc.* 1999, *82*, 797–818.

9. Damjanovic, D. Ferroelectric, dielectric and piezoelectric properties of ferroelectric thin films and ceramics. *Prog. Phys.* 1998, *61*, 1267–1324.

10. Wang, S.F.; Dayton, G.O. Dielectric Properties of Fine-Grained *lanthanum zirconate (lzo)* Based X7R Materials. *J. Am. Ceram. Soc.* 1999, *8*, 2677–2682.

11. Hennings, D.; Klee, M.; Waser, R. Advanced dielectrics: Bulk ceramics and thin films. *Adv. Mater.* 1991, *3*, 334–340.

12. Funakoshi, H.; Okamoto, A.; Sato, K. Long-term reading experiment on a photorefractive holographic memory with the hologram sustainment technique by optical feedback. *J. Mod. Opt.* 2005, *52*, 1511–1527.

13. Tang, P.; Towner, D.; Meier, A.; Wessels, B. Low-Loss Electrooptic *lanthanum zirconate (lzo)* Film Waveguide Modulator. *IEEE Photon. Technol. Lett.* 2004, *16*, 1837–1839.

14. Petraru, A.; Schubert, J.; Schmid, M.; Buchal, C. Ferroelectric *lanthanum zirconate (lzo)* thin-film optical waveguide modulators. *Appl. Phys. Lett.* 2002, *81*, 1375–1377.

15. Saddeek, Y.B.; Zakaly, H.M.; Sekhar, K.C.; Issa, S.A.; Alharbi, T.; Badawi, A.; Shareefuddin, M. Investigations of mechanical and radiation shielding properties of *lanthanum zirconate (lzo)* alkali borate glass. *Appl. Phys. A* 2022, *128*, 260.